JPIChE 54 (2) 2026: 01-12

PAKISTAN INSTITUTE OF CHEMICAL ENGINEERS
Since 1969

Journal of the Pakistan Institute of Chemical Engineers
Journal homepage: www.piche.org.pk/journals

DOI: https://doi.org/10.54693/piche.05421

Check for updates

Rational Design of Functionalized Ionic Liquids for Silica Gel Suppression during Leaching of Coal Fly Ash: COSMO-RS guided Screening

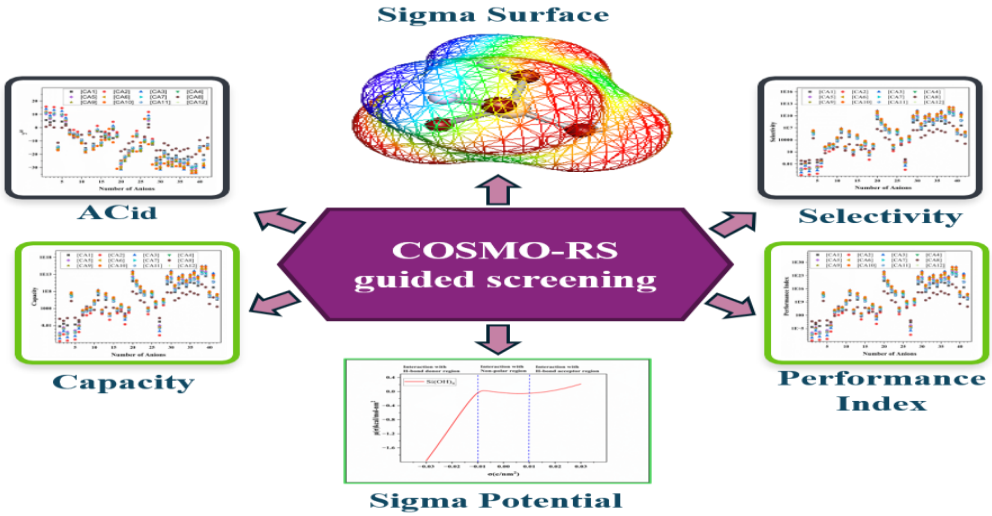
A. Mehmood[1], A.S. Maulud[1*], M. Nawaz[1], M.A. Bustam[1], N.E. Rabat[1], Y. Jamal[2]

Submitted: 16/07/2026, Accepted: 22/09/2026, Published: 29/09/2026

ABSTRACT

Ionic liquids (ILs) have attracted considerable attention as green, tunable solvents for hydrometallurgical processes. Coal fly ash (CFA) has emerged as a promising secondary resource of rare earth elements (REEs). However, during conventional solvent leaching of rich-silica CFA, dissolved silica polymerizes into a dense gel. This silica gelation entraps liberated REEs, increases viscosity, and causes filtration obstructions, presenting a major bottleneck for efficient REE recovery. To overcome this challenge, specifically designed ILs can hinder gelation by interacting with monomeric silicic acid. Because testing millions of possible cation-anion combinations by trial and error is practically unfeasible and resource-intensive, a predictive computational framework is required. In this study, the conductor-like screening model for real solvents (COSMO-RS) was applied to computationally pre-screen 504 IL combinations, derived from 12 cations and 42 anions, for their thermodynamic affinity toward silicic acid. The potential efficacy of each IL design was evaluated based on activity coefficients, selectivity, capacity, and performance index. Specifically, tetrabutylammonium citrate (CA3, AN39), tetrabutylammonium oxalate (CA3,AN38), 1-butyl-1-methylpyrrolidinium acetate (CA10, AN20) emerged as the most efficient formulations among the 504 investigated ILs for suppressing silica gelation. This framework provides a rational, molecular-level blueprint for selecting ILs that suppress silica gelation, thereby enabling efficient hydrometallurgical recycling of industrial waste.

Keywords: Activity coefficient, Coal fly ash, COSMO-RS, Ionic liquids, Selectivity, Performance Index



Graphical Abstract

[1] Department of Chemical Engineering, Universiti Teknologi PETRONAS, Perak, Malaysia.
[2] Institute of Chemical Engineering and Technology, University of the Punjab, Lahore, Pakistan.
***Correspondence Author:** Abdulhalim Shah Maulud (halims@utp.edu.my)

1. Introduction:

A key component of the contemporary circular economy is the sustainable management and value-adding of industrial byproducts. Among these, coal fly ash (CFA) waste stream generated from coal power plants presents a severe environmental liability, with a total annual production of 1.63 billion tons produced globally [1]. Despite its reuse potential, less than half of this volume is currently utilized in secondary applications such as cement, ceramics, bricks and concrete, with the vast majority still relegated to landfills [2]. However, CFA is enriched in critical materials and valuable metals, including aluminium, iron, titanium, and rare earth elements (REEs) [3, 4]. Owing to its high content of aluminosilicate glass and silica-rich mineral phases, CFA has recently attracted significant attention as a strategic secondary resource for critical mineral recovery via hydrometallurgical processing [5, 6].

The conventional hydrometallurgical treatment of CFA generally relies on mineral acids and alkaline leaching. During this process, aluminosilicate phases decompose, causing amorphous silica to readily dissolve into the solution to form monomeric silicic acid (H_4SiO_4) [7]. As its concentration surpasses critical thermodynamic thresholds, these monomers undergo complex polymerization and condensation reactions. The silicic acid molecules condense to form siloxane (Si–O–Si) bonds, generating polymeric silica networks that rapidly evolve into three-dimensional amorphous silica gel [8].

In high-silicon resource hydrometallurgy, silica gel production poses operational issues. The gelation increases viscosity, blocks filtration media, and halts downstream separation and purification processes [9]. Likewise, the gel matrix physically entraps dissolved metal species, causing process inefficiencies, poor operational reproducibility, and major technical hurdles for large-scale commercialization [10]. Traditional mitigation strategies, including pulp ageing [11], thermal dehydration [12] and the addition of sacrificial flocculants, frequently suffer from high energy consumption, chemical requirements and poor selectivity [13]. Alternative process modifications, such as optimizing acid concentration, operating temperature, liquid-to-solid ratio, time, additives, and staged leaching, can reduce gelation within narrow operating windows. However, these methods rely on empirical optimization, elevate chemical consumption, and require complex process controls [14]. Notably, they do not address the fundamental, molecular-level solvent-solute interactions that govern silica dissolution and polymerization [15]. Consequently, more sophisticated chemical interventions are needed.

Over the last few years, Ionic liquids (ILs) have emerged as promising alternative solvents owing to their negligible vapor pressure, exceptional thermal and chemical stabilities, and tunable physicochemical properties [16]. By independently pairing different cations and anions, ILs can be rationally designed to exhibit targeted polarities and hydrogen-bonding capabilities. This structural flexibility provides an opportunity to tailor IL- silicic acid interactions. Specific combinations of IL cations and anions can interact strongly with silanol groups (Si-OH) via hydrogen bonding or electrostatic forces. These interactions can cap active polymerization sites. Consequently, the structural evolution of the siloxane (Si-O-Si) framework can be suppressed [17]. However, the vast number of possible cation-anion pairings enables the design of millions of IL formulations. Rigorous pre-screening of their thermodynamic properties is necessary to identify suitable candidates before experimental realization. The Conductor-like Screening Model for Real Solvents (COSMO-RS) has emerged as a reliable predictive tool [18]. COSMO-RS effectively models solvent-solute interactions and pre-screens target reagents from quantum chemical descriptors, significantly reducing the time, cost, and resources associated with traditional trial-and-error experiments [19].

In this work, COSMO-RS has been employed to design and screen ILs based on their thermodynamic affinity for monomeric silicic acid. Silicic acid was chosen as a representative target solute because blocking its initial self-condensation and polymerization stages is the key to preventing macroscopic gel network formation [20]. To the best of our knowledge, no previous study has systematically used COSMO-RS screening to design ILs to inhibit silica gel formation during CFA leaching. This study bridges the gap by integrating molecular-level thermodynamic screening. To accomplish this, a diverse set of 504 ILs was constructed by pairing 12 representative cation families (choline, ammonium, betaine, imidazolium, pyridinium, piperidinium and pyrrolidinium) with 42 distinct anions. Additionally,

thermodynamic properties, including activity coefficients (γ^{id}) at infinite dilution, capacity, selectivity, and performance index (P.I.), were computed to elucidate molecular-level interactions between the ILs and silicic acid. Finally, this work aims to identify high-performance ILs capable of strong interaction with silicic acid for potential silica gelation mitigation during the leaching of silica-rich CFA, offering a sustainable and effective alternative to conventional hydrometallurgical leaching systems.

2. Materials and Methods:

2.1. COSMO-RS Computational Methodology:

This study employs the COSMO-RS-guided framework to investigate the interactions between selected ILs and silicic acid, with the aim of suppressing silica gel for potentially enhance leaching efficiency from CFA. COSMO-RS is a powerful and efficient screening software capable of evaluating a large number of solvents for specific solutes [21]. COSMO-RS estimates macroscopic thermodynamic properties of liquid systems by statistically evaluating intermolecular interactions derived from quantum-chemical COSMO surface segment calculations [22, 23].

All simulations were carried out using the COSMOtherm software (version 19.0.1, Germany). Initially, the COSMO-RS library was consulted to verify the structural availability of the compounds investigated in this study. For geometry optimization, the structures of the solute (silicic acid), cations, and anions were constructed using the Turbomole graphical interface (TmoleX, Version 4.4.1.). The structures were subjected to a self-consistency algorithm (SCF) calculation for optimization with Becke-Perdew theory and the def_2-TZVP as basis set [24]. Subsequent COSMO-RS thermodynamic calculations were conducted under standard operating conditions of 298.15 K and 1.013 bar.

In COSMO-RS computations for IL-$Si(OH)_4$ systems, the “electroneutral mixture (pseudo-binary) approach” was employed, in which the IL cation and anion were tested as independent species with equal mole fractions [25]. This approach has been reported as well-established for its high predictive accuracy, consistently reproducing experimental trends across diverse chemical systems [26]. The stable conformers of cations and anions were selected for the following COSMO-RS calculations. Based on the optimized structure of $Si(OH)_4$, σ-profiles, σ-potentials, activity coefficients (AC_id), selectivity, capacity, and performance index were evaluated to assess the appropriateness of the ILs as leaching agents.

The selection of the 12 cations and 42 anions (yielding 504 IL combinations) followed a systematic, multi-criteria rationale tailored to hydrometallurgical applications. Cations were selected from diverse structural classes, including quaternary ammoniums, imidazolium, pyridiniums, piperidiniums, pyrrolidiniums, and choline/betaine derivatives. This diversity enabled systematic evaluation of the effect of alkyl chain length, charge delocalization, and steric hindrance on silicic acid binding. Similarly, the anions were selected to cover a broad range of hydrogen-bond-accepting capabilities. These ranged from non-coordinating hydrophobic fluorinated species to highly polar and coordinating functional groups, including carboxylates, sulfates, phosphates, and amino acid derivatives. The screening framework also considered important constraints related to industrial scale-up. These included commercial availability, ease of synthesis, chemical stability, and low environmental toxicity. Bio-derived choline, betaine, and amino acid anions were included in this context. Balanced hydrophilicity was also considered to minimize phase entrainment during leaching. Fig. 1 presents a schematic overview of the COSMO-RS computational workflow used in this study.

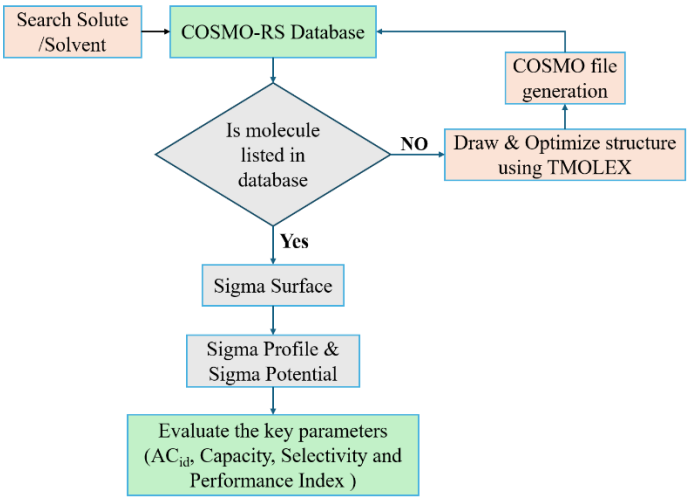


Figure 1: Systematic methodology for COSMO-RS

2.2. Sigma Profile (σ) and Sigma Potential (σ):

The **σ** profiles of the solute are calculated using the equation (1) [21].

$$\rho_{i(\sigma)} = \frac{\Sigma_i x_i n_i \rho_i(\sigma)}{\Sigma_i x_i n_i} = \Sigma_i^N x_i \rho_i(\sigma) \quad (1)$$

Where $x\,i$ is the concentration of $Si(OH)_4$.

The σ-profiles were used to qualitatively assess possible interaction modes between $Si(OH)_4$ and the investigated solvents, such as π–π interactions, hydrogen bonding, and hydrophilic effects, which contribute to improved solubility.

2.3. Activity Coefficient at Infinite Dilution (γ^{id}):

The γ^{id} of the interaction of silicic acid (solute) in ILs was computed according to the equation (2) [27]:

$$\gamma = exp\left(\frac{\mu - \mu^0}{RT}\right) \quad (2)$$

The symbols μ correspond to the chemical potential of the IL, while μ^0 corresponds to the chemical potential of the solute [28].

2.4. Capacity and Selectivity:

The bonding strength of the IL is donated by the capacity explained in equation (3) [29]:

$$Capacity = \left(\frac{1}{AC^{id}}\right)^{IL\,Phase} \quad (3)$$

Selectivity (S^{id}), which reflects the ability of a solvent to preferentially extract a target solute [30]. The representation of selectivity is described in equation (4) [21]:

$$S^{id} = \left(\frac{AC^{id_2}}{AC^{id_1}}\right)^{IL\,phase} \quad (4)$$

The subscripts 1 and 2 represent water and solute ($Si(OH_4)$), respectively.

2.5. Performance Index (P.I.):

In addition to S^{id}, the P.I. at infinite dilution was evaluated to identify the most promising solvent for experimental validation [31]. This P.I. serves as an integrated criterion for assessing the suitability of solvents for further application, as defined in equation (5) [32]:

$$P \cdot I = C^{id} \times S^{id} = \left(\frac{AC^{id_2}}{(AC^{id1})^2}\right) \quad (5)$$

To select the final recommended ILs, the calculated thermodynamic descriptors were evaluated collectively using a hierarchical screening approach:

Initial screening: Candidates were first filtered to identify ILs displaying low activity coefficients (γ^{id}) and high capacity for silicic acid.

Trade-off Optimization: To address inherent trade-offs between extraction capacity and selectivity, the performance index (P.I = C^{id} * S^{id}) was applied as the primary unified ranking metric.

ILs composed of 12 cations and 42 anions were screened by the COSMO-RS, as provided in the supplementary file Table S1 and Table S2.

3. Results and Discussion:

3.1. Sigma surface of $Si(OH)_4$:

The charge distribution, polarity, and bonding characteristics of $Si(OH)_4$ were evaluated using the three-dimensional (3D) σ-surface generated through COSMO-RS. The σ-surface of $Si(OH)_4$ is presented in Fig.2. The color spectrum mapping the topography of the σ-surface serves as a visual indicator of localized chemical potentials and intermolecular coordination sites. Specifically, the red regions identify highly electronegative domains with strong hydrogen-bond-accepting capabilities, while the yellow zones denote partially electronegative, weakly coordinating areas. The green segments represent chemically inert, neutral, non-polar surfaces. The prominent blue regions highlight electropositive domains localized over the hydroxyl protons, emphasizing the strong hydrogen-bond-donating character of the silanol groups [33]. This detailed electrostatic mapping provides the fundamental molecular rationale for the high affinity of $Si(OH)_4$ toward polar, oxygenated IL anions capable of forming cooperative hydrogen-bonded networks.

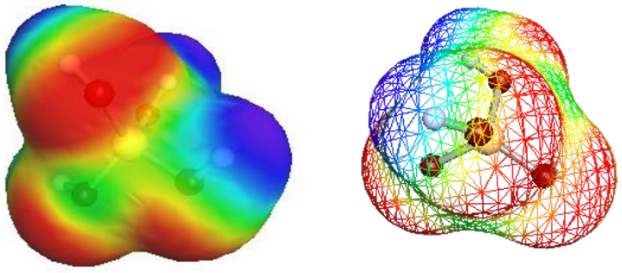


Figure 2: σ Surface of $Si(OH)_4$ predicted using the COSMO-RS.

3.2. Sigma profile of $Si(OH)_4$:

The σ-profile provides insight into the polarity and bonding characteristics of the molecule under investigation and serves as a useful descriptor for understanding its intermolecular interactions with solvents [34]. This representation reflects the distribution of polar and non-polar surface regions of the molecule, thereby offering qualitative information on its interaction potential. In a σ-profile plot, the horizontal

axis corresponds to the surface charge density, whereas the vertical axis represents the fraction of the molecular surface associated with each charge density interval. The resulting peaks indicate surface regions with different electron density characteristics, enabling the identification and comparison of polar or non-polar. The σ-profile can be interpreted across three functional domains: the hydrogen-bond donor (HBD) region < -0.01, the hydrogen-bond acceptor (HBA) region > +0.01, and the central non-polar region -0.01 < σ > +0.01 [33].

As illustrated in Fig. 3, the σ profile peaks of $Si(OH)_4$ exhibit lower intensity peaks within the non-polar region, indicating its polar nature. Consequently, $Si(OH)_4$ is expected to exhibit stronger interactions with solvents possessing high polarity. Furthermore, prominent peaks are observed in the HBA region, with comparatively lower peaks in HBD region, indicating the potential of $Si(OH)_4$ to be attracted towards ILs with HBA properties. The sharp peaks at 0.012 e/nm^2 and 0.016 e/nm^2 further indicate the ability of $Si(OH)_4$ to act as a strong HBA. Overall, these results suggest that $Si(OH)_4$ has hydrogen bond accepting and donating characteristics.

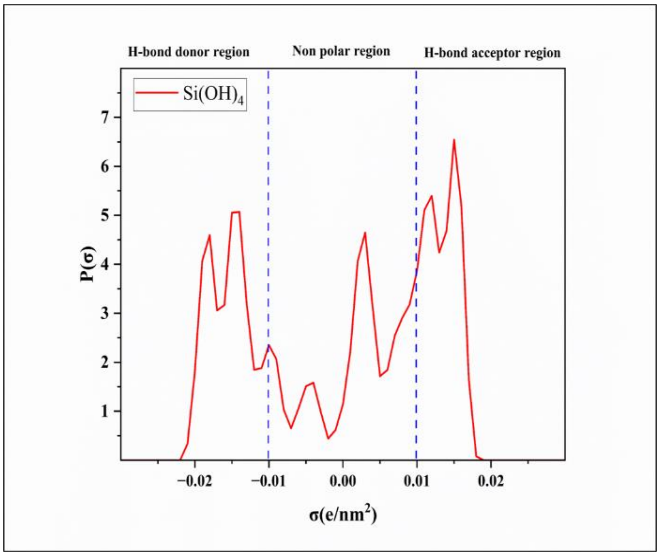


Figure 3: Sigma profiles of $Si(OH)_4$ computed by COSMO-RS

3.3. Sigma potential of $Si(OH)_4$:

The sigma potential describes the variation of the chemical potential of a compound's surface as a function of screening charge density, thereby providing insight into the electrostatic interaction capability of the compound surface toward ILs. This parameter is derived from the sigma profile and is regarded as a thermodynamic property [35]. In the corresponding plot, the horizontal axis represents the surface charge density, expressed in e/nm^2, while the vertical axis denotes the sigma potential.

As shown by the σ potential distribution in Fig. 4, positive values of μ(σ) correspond to unfavorable or repulsive interactions upon molecular contact, whereas negative values indicate energetically favorable chemical interactions [28]. Pronounced negative σ-potential values are observed in the HBD interaction region, suggesting that $Si(OH)_4$ can form favorable interactions with ILs exhibiting complementary hydrogen-bonding characteristics. In contrast, comparatively less negative μ(σ) values are observed in the HBA region, indicating weaker interactions in this domain. In this framework, σ < −0.01 e/nm^2 corresponds to the HBD region, σ > +0.01 e/nm^2 represents the HBA region, and −0.01 < σ < +0.01 e/nm^2 is associated with non-polar region [36].

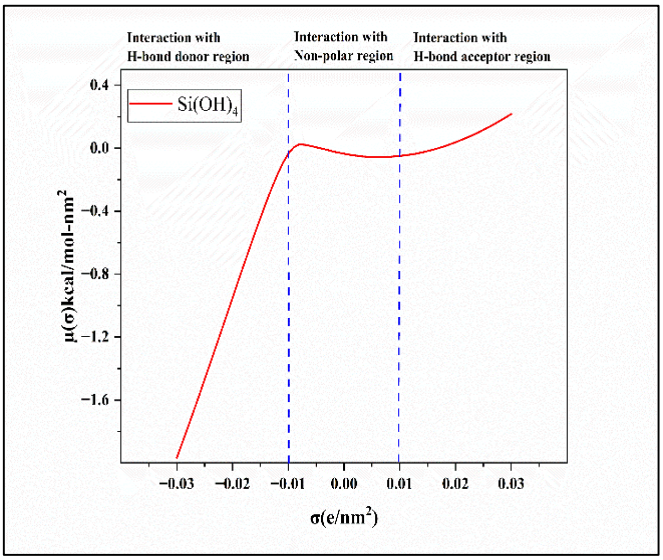


Figure 4: Sigma potential of $Si(OH)_4$ computed by COSMO-RS

Overall, the combined σ-profile and σ-potential analyses suggest that silicic acid interacts more strongly with ILs possessing hydrogen-bond-donating functionalities, while weaker interactions with ILs are dominated by hydrogen-bond-acceptor ability. Moreover, these results indicate that ILs featuring both hydrogen-bond-donating and accepting sites, together with minimal polar character, are particularly suitable candidates for interaction with $Si(OH)_4$, ultimately have the potential to suppress the silica gel during leaching with silica-rich CFA.

3.4. Activity Coefficient at infinite dilution (γ^{id}):

A basic thermodynamic descriptor for assessing the intermolecular affinity between ILs and a solute is the γ^{id}. Stronger interactions between silicic acid and ILs are indicated by lower γ^{id} values in hydrometallurgical processes. This coordination wraps the monomeric silicic acid in a protective solvation shell, effectively capping the silanol functional groups and preventing the spontaneous condensation cross-linking that drives silica gelation. Consequently, suppressing the physical gel barrier preserves fluid mass transfer and enhances leaching efficiency. Conversely, higher γ^{id} values reflect weak IL–solute coordination, leaving the silicic acid monomers thermodynamically free to polymerize rapidly into a dense gel-like matrix.

The COSMO-RS-guided γ^{id} of silicic acid in 504 ILs with twelve cations and forty-two different anions is shown in Figure 5. The wide variance in γ^{id} values underlines a high sensitivity to structural pairing, allowing for systematic screening based on cation core taxonomy: (a) quaternary ammonium, (b) imidazolium-based, (c) pyridinium-based, and (d) saturated heterocyclic cations. Mechanistically, the screening shows that cation-dependent affinity follows the order: quaternary ammonium > saturated heterocyclic > pyridinium > imidazolium-based systems. The most favorable thermodynamic interactions are dominated by the symmetrically branched tetra-n-butylammonium (CA3) paired with multi-dentate organic carboxylates like citrate (AN39) and oxalate (AN38), which yield the lowest overall γ^{id} values. This peak performance is driven by a cooperative balance where localized negative charge densities on the carboxylate oxygen engage in dense hydrogen-bonding networks with the silanol protons, while the complementary dispersion forces and localized alkyl conformation of (CA3) shield the complexes from self-aggregation. Similarly, among the saturated cyclic architectures, 1-butyl-1-methylpyrrolidinium (CA10) exhibits exceptionally low γ^{id} values when combined with the highly basic lysinate (AN29) and the charge-localized ethyl sulfate (AN19). This confirms that pairing localized, low-steric heterocyclic cations with strong hydrogen-bond-accepting anions creates an optimal thermodynamic sink for monomeric silica, marking these combinations as promising candidates predicted to inhibit silica gel formation during acid leaching.

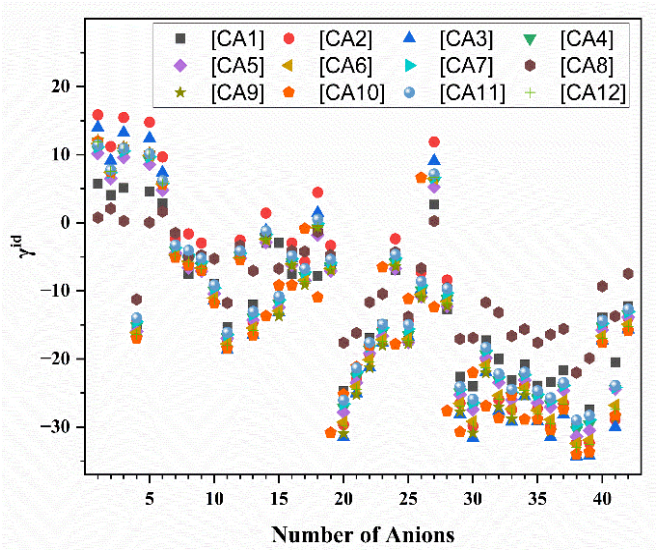


Figure 5: γ^{id} at infinite dilution of Si(OH)4 as anticipated by COSMO-RS at 298.15 K.

3.4. Capacity at infinite dilution of ILs:

The thermodynamic capacity of the IL phase toward the silicic acid solute was calculated using COSMO-RS in order to assess the performance of the designed ILs (Fig. 6). The resulting capacity profile reveals a strong dependence on the charge density and coordinating ability of the anion. Specifically, highly fluorinated and bulky halide-based anions, including tris(pentafluoroethyl)trifluorophosphate (AN1), tetrachloroborate (AN5), hexafluorophosphate (AN27), and triiodide (AN3), exhibit remarkably poor capacity toward the polar silicic acid when paired with hydrophobic, sterically hindered cations like tetraoctylammonium (CA2) and tetra-n-butylammonium (CA3). Thermodynamically, this poor capacity stems from the weakly coordinating nature and highly delocalized charge of these fluorinated species, which fail to establish favorable hydrogen-bonding networks with the silanol groups of the solute [37]. This behavior directly mirrors the trends observed in the γ^{id} calculations, where the pairing of (CA3) with highly fluorinated anions like (AN1) and (AN5) yielded unfavorable activity coefficients, confirming their inability to stabilize monomeric silicic acid.

On the other hand, among all the anions under investigation, the organic carboxylate anions oxalate (AN38), citrate (AN39), and acetate (AN20) demonstrated a high capacity for silicic acid. Regardless of the coupled cation, the highest capacity was attained by the hydrophilic citrate (AN39). This performance is

primarily driven by the high hydrogen-bond acceptor capacity of the citrate anion's carboxylate groups; it possesses both strongly polar regions (three carboxylate groups and a central hydroxyl group) capable of establishing dense, multidentate hydrogen-bonding chelates with silicic acid, and a short, non-polar carbon backbone that balances the electrostatic field of the system [38]. This polar synergy maximizes the solvation shell density around the silicic acid, proving that carboxylate-functionalized ILs provide a thermodynamic sink to inhibit silica gel and sustain high rare earth leaching efficiencies.

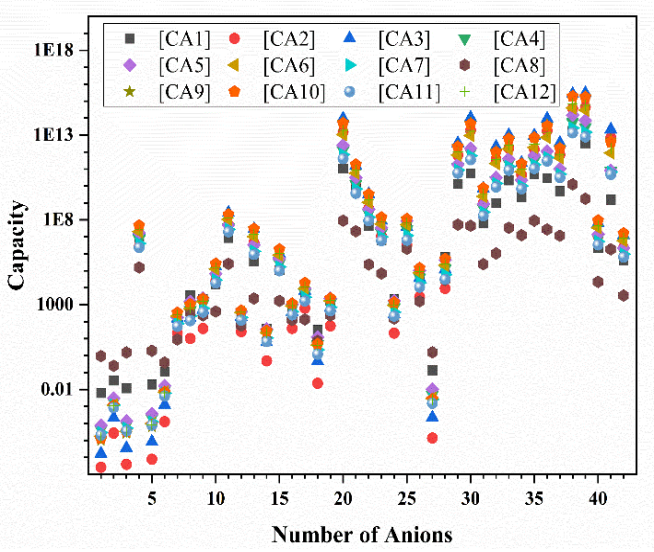


Figure 6: Capacity of ILs for Si(OH)4 as anticipated by COSMO-RS at 298.15 K.

3.5. Selectivity at infinite dilution of ILs:

The thermodynamic selectivity for the silicic acid solute was calculated over all 504 IL combinations using COSMO-RS to assess the affinity of the IL solvents in a complex leaching matrix (Fig. 7). The screening reveals that carboxylate-functionalized anions, specifically oxalate (AN38), citrate (AN39), and acetate (AN20) in combination with the tetra-n-butylammonium (CA3) and 1-butyl-1-methylpyrrolidinium (CA10) cations demonstrate the highest selectivity for silicic acid. Conversely, the lowest selectivity values were recorded by the hydrophobic pairings, namely (CA2, AN1), (CA2, AN3), and (CA2, AN5). This bifurcation in selectivity follows the thermodynamic principle of "like dissolves like." As demonstrated by the screening, these latter combinations possess highly non-polar, weakly coordinating characteristics that create a severe phase mismatch with the solute. This behavior aligns with the complementary sigma profile analysis (Fig. 3), which establishes that monomeric silicic acid is a predominantly polar molecule characterized by dense hydrogen-bond-donating silanol groups. Consequently, non-polar ILs exhibit minimal interaction and negligible selectivity toward the hydrophilic solute.

Additionally, as the structural distribution plots (Fig. 6) demonstrate, the cation's alkyl chain length and structural arrangement have a significant impact on bonding capabilities. Cations containing an aromatic core, such as 1-ethyl-3-methylimidazolium (CA5), 1-butyl-3-methylimidazolium (CA4), and 1-butyl-2-methylpyridinium (CA6), exhibit a moderate selectivity window for silicic acid due to the aromatic structure, resulting in charge delocalization and steric hindrance [39]. These findings underscore that optimizing the spatial configuration and charge density of the IL components is crucial for maximizing solute selectivity. The targeted ILs interact strongly with silicic acid, which is predicted to mitigate polymerization and facilitate REE recovery.

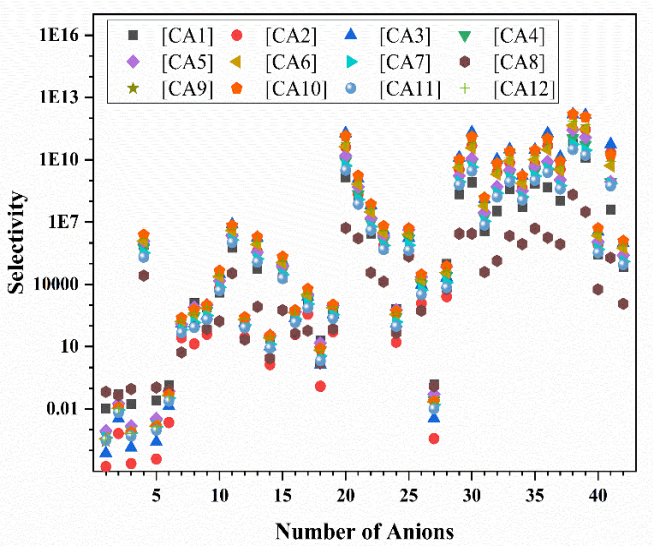


Figure 7: Selectivity of ILs for Si(OH)4 as anticipated by COSMO-RS at 298.15 K.

3.6. Performance Index (P.I):

To systematically screen IL candidates and choose the most promising ones for experimental validation, the P.I. was calculated using COSMO-RS [21]. As shown in Fig. 8, the P.I. profile across the 504 screening ILs depends on anion polarity and charge density. The optimum P.I. values are exclusively dominated by highly polar, oxygenated anions, specifically oxalate (AN38), citrate (AN39), acetate (AN20), propanoate (AN30), and

leucinate (AN37), regardless of the paired cation. In contrast, weakly coordinating, non-polar anions such as tris(pentafluoroethyl) trifluorophosphate (AN1), triiodide (AN3), tetrachloroborate (AN5), and hexafluorophosphate (AN27) consistently recorded the lowest P.I. scores. This performance deficit is structurally driven by the bulky, delocalized nature of these fluorinated and heavy-halide architectures, which lack the localized hydrogen-bond-accepting domains required to interact with the polar silanol groups of monomeric silicic acid. Among the screened cations, quaternary ammonium-based systems yielded the highest overall P.I., highlighting the immense potential of these functional IL architectures for silica gel inhibition.

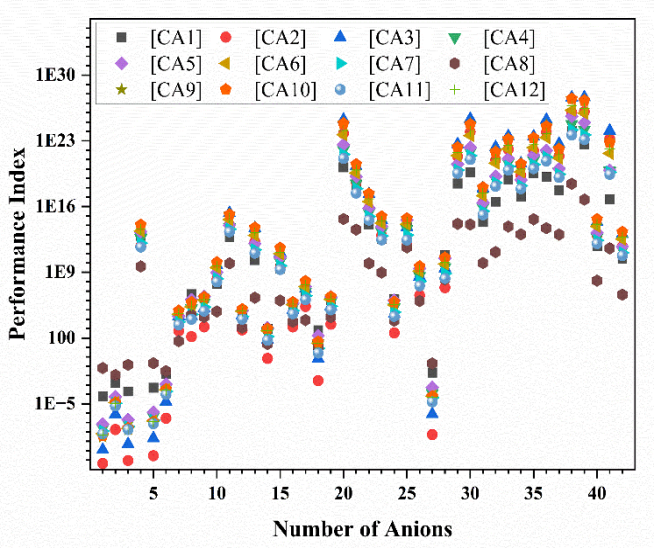


Figure 8: P.I of ILs for Si(OH)4 as anticipated by COSMO-RS at 298.15 K.

To further contextualize these findings, high-performing IL candidates, particularly (CA3, AN38) and (CA3, AN39), were compared with conventional IL families that have been widely investigated for rare earth element extraction and related hydrometallurgical applications [40, 41]. For example, imidazolium-based ILs containing bis(trifluoromethylsulfonyl) imide (NTf_2) anions have received considerable attention because of their hydrophobicity, thermal stability, and favorable physicochemical properties [40]. Similarly, quaternary ammonium-based ILs and chloride-containing systems have been explored as extractants and processing media in hydrometallurgical applications. However, these conventional ILs are generally designed to facilitate metal extraction, phase separation, or the dissolution of specific metal species rather than to promote strong and cooperative interactions with highly hydroxylated silica species. Consequently, the present results suggest that targeted anion functionalization represents an important design strategy for developing ILs specifically tailored for silicic acid management. Thus, whereas previously reported ILs have primarily been optimized for metal extraction in hydrometallurgical systems, the IL candidates identified in this study are computationally designed to address silica-related challenges, providing a complementary approach that may be particularly relevant for complex feedstocks such as coal fly ash [16].

Table 1 summarizes the highest-performing ILs and their corresponding thermodynamic parameter values.

Table 1. COSMO-RS-based summary of the highest-performing ILs and their calculated activity coefficient, selectivity, capacity, and performance index values.

Sr. No.	ILs	Activity Coefficient	Capacity	Selectivity	Performance Index
1	(CA3,AN39)	-34.24427	2.9796 x 10^{15}	1.4188 x 10^{12}	4.22746 x 10^{27}
2	(CA3,AN38)	-34.30121	2.6412 x 10^{15}	1.5232 x 10^{12}	4.02308 x 10^{27}
3	(CA10,AN20)	-25.23273	5.0092 x 10^{13}	1.3905 x 10^{11}	6.96529 x 10^{24}
4	(CA10,AN30)	-22.0276	4.5008 x 10^{13}	1.2517 x 10^{11}	5.63365 x 10^{24}

While thermodynamic descriptors pinpoint a broad library of high-performing candidates, transitioning from screening to practical hydrometallurgical application requires a balanced evaluation of economic and process constraints. Considering criteria such as production costs, commercial availability, ease of synthesis, stripping efficiency, and robust structural regeneration, the combination of tetra-n-butylammonium (CA3) with oxalate (AN38) and citrate (AN39) was assigned the highest priority for implementation. Thermodynamically, the polar nature of these quaternary ammonium salts creates an ideal electronic environment for establishing dense, cooperative hydrogen-bonding networks that stabilize silicic acid and preclude condensation polymerization.

The computational findings provide a rational framework to guide future experimental investigations. By leveraging COSMO-RS simulations to screen 504 IL combinations, the identified promising IL candidates can be prioritized for laboratory validation, thereby reducing the required experimental search space. Future studies

could focus on experimental validation by synthesizing the promising ILs and characterizing their direct interactions with silicic acid using complementary spectroscopic techniques such as UV-Vis and FTIR. Furthermore, their practical effectiveness could subsequently be assessed during coal fly ash leaching by monitoring silica dissolution and silica gel formation, together with the recovery of rare earth elements. While this screening establishes candidates with high intrinsic affinity for silicic acid mitigation, validating selectivity within realistic, multicomponent CFA leaching media containing competing metal species (Al^{3+}, Fe^{3+}, Ca^{2+}, Ti^{4+}) remains a vital next step toward practical implementation.

4. Conclusion:

This study used COSMO-RS as a predictive thermodynamic framework to evaluate 504 IL combinations (12 cations and 42 anions) to inhibit silica gel during CFA leaching. The computational screening revealed that the quaternary ammonium cation tetra-n-butylammonium (CA3) and the saturated heterocyclic 1-butyl-1-methylpyrrolidinium cation (CA10) serve as the most effective co-solvent architectures when paired with strongly hydrophilic, oxygenated anions. Explicitly, tetrabutylammonium citrate (CA3, AN39), tetrabutylammonium oxalate (CA3, AN38), 1-butyl-1-methylpyrrolidinium acetate (CA10, AN20), and 1-butyl-1-methylpyrrolidinium propanoate (CA10, AN30) emerged as the potential formulations for suppressing silica gelation. Thermodynamically, these high-performing ILs yielded low activity coefficients at infinite dilution γ^{id}, which translated directly to high capacity, selectivity, and performance index (P.I.) profiles for the monomeric silicic acid solute. This peak performance is driven by dense, cooperative hydrogen-bonding networks that efficiently cap the silanol functional groups, leaving no structural opportunity for spontaneous condensation polymerization. In contrast, ILs incorporating bulky, weakly coordinating fluorinated and halide-based anions such as tris(pentafluoroethyl) trifluorophosphate (AN1), triiodide (AN3), tetrachloroborate (AN5), bis(trifluoromethylsulfonyl) imide (AN6), and hexafluorophosphate (AN27) proved inefficient due to thermodynamic phase mismatch with the polar solute. While both the citrate (AN39) and oxalate (AN38) anions demonstrated outstanding stabilization performance, the citrate-based ILs were assigned the highest priority for practical implementation due to their superior economic feasibility and industrial viability. Ultimately, this work provides a molecular-level foundation for designing target-specific ILs to mitigate silica gelation, offering critical engineering insights needed to scale up hydrometallurgical REE recovery processes.

Acknowledgement

The authors acknowledge the funding support provided by Yayasan Universiti Teknologi PETRONAS (YUTP) through Cost Centre 015LC0-545. The authors would also like to acknowledge the Department of Chemical Engineering at Universiti Teknologi PETRONAS for their support and contributions to this research.

Declaration of Competing Interest

The authors declare that they have no known competing financial or personal interests.

References

[1] J. Jiang *et al.*, "Highly activated pozzolanic materials to develop sustainable concrete: a new perspective from photoexcited nano-TiO2," *Cement and Concrete Composites,* vol. 162, p. 106149, 2025/09/01/ 2025, doi: https://doi.org/10.1016/j.cemconcomp.2025.106149.

[2] N. Gupta, V. V. Gedam, C. Moghe, and P. Labhasetwar, "Investigation of characteristics and leaching behavior of coal fly ash, coal fly ash bricks and clay bricks," *Environmental Technology & Innovation,* vol. 7, pp. 152-159, 2017/04/01/ 2017, doi: https://doi.org/10.1016/j.eti.2017.02.002.

[3] N. Ünal-Kartal, "Rare Earth Elements in Turkish Coal Fly Ashes: Enrichment Patterns and Secondary Resource Perspective," *Sustainability (Switzerland),* Article vol. 18, no. 5, 2026, Art no. 2529, doi: 10.3390/su18052529.

[4] M. Imran, K. Shahzad, S. Munir, M. Wasim, and A. Hussnain, "Synthesis and characterization of potassium silicate fertilizer using fly ashes of bituminous and sub-bituminous and lignite coal," *Journal of the Pakistan Institute of Chemical Engineers,* vol. 48, no. 2, pp. 47-54, 2020.

[5] D. K. Rajak, S. Suman, C. Guria, and G. Kumar, "Sustainable Utilization of Anthropogenic Coal Fly Ash Through Mechanical and Chemical Activation," in *Anthropogenic Environmental*

Hazards: Compensation and Mitigation, 2023, pp. 143-159.

[6] A. Mehmood, N. Haleem, M. Yaseen, Y. Jamal, and M. Safwan, "Sulfur recovery from lignite coal and desulfurization solution for environmental sustainability," *International Journal of Coal Preparation and Utilization,* vol. 46, no. 3, pp. 727-740, 2026/03/04 2026, doi: 10.1080/19392699.2025.2473413.

[7] L. Xing, X. Li, P. Cao, J. Luo, and H. Jiang, "Stepwise extraction and utilization of silica and alumina from coal fly ash by mild hydrothermal process," *Process Safety and Environmental Protection,* Article vol. 182, pp. 918-929, 2024, doi: 10.1016/j.psep.2023.12.035.

[8] D. J. Belton, O. Deschaume, S. V. Patwardhan, and C. C. Perry, "A solution study of silica condensation and speciation with relevance to in vitro investigations of biosilicification," *Journal of Physical Chemistry B,* Article vol. 114, no. 31, pp. 9947-9955, 2010, doi: 10.1021/jp101347q.

[9] Q. Lu *et al.*, "Advances in tuning the filtration performance of the ore pulp during hydrometallurgical leaching of high-silicon materials: A review," *Minerals Engineering,* Review vol. 244, 2026, Art no. 110259, doi: 10.1016/j.mineng.2026.110259.

[10] J. F. King, R. K. Taggart, R. C. Smith, J. C. Hower, and H. Hsu-Kim, "Aqueous acid and alkaline extraction of rare earth elements from coal combustion ash," *International journal of coal geology,* vol. 195, pp. 75-83, 2018.

[11] S. Iswar, W. J. Malfait, S. Balog, F. Winnefeld, M. Lattuada, and M. M. Koebel, "Effect of aging on silica aerogel properties," *Microporous and Mesoporous Materials,* Article vol. 241, pp. 293-302, 2017, doi: 10.1016/j.micromeso.2016.11.037.

[12] Y. Li *et al.*, "Recent Progress of Multifunctional Silica Aerogel Composite Materials: From Fabrication Strategies to Versatile Applications," *ACS Applied Materials and Interfaces,* Review vol. 17, no. 23, pp. 33296-33317, 2025, doi: 10.1021/acsami.5c00606.

[13] D. Pietras-Ożga *et al.*, "Chapter 9 - Sol-gel–derived silica xerogels: Synthesis, properties, and their applicability for removal of hazardous pollutants" in *Advanced Materials for Sustainable Environmental Remediation*, D. Giannakoudakis, L. Meili, and I. Anastopoulos Eds.: Elsevier, 2022, pp. 261-277.

[14] W. Zhang, Y. Yao, B. He, and R. Wang, "The energy-saving characteristic of silica gel regeneration with high-intensity ultrasound," *Applied Energy,* Article vol. 88, no. 6, pp. 2146-2156, 2011, doi: 10.1016/j.apenergy.2010.12.023.

[15] L. Wang *et al.*, "Two-stage method recovery of metals from copper slag: Realize the resource utilization of all components," *Minerals Engineering,* vol. 206, p. 108503, 2024/01/01/ 2024, doi: https://doi.org/10.1016/j.mineng.2023.108503.

[16] D. Asubonteng *et al.*, "Leaching enhancement of rare earth elements from ion adsorption clay using choline acetate and betaine hydrochloride," *Journal of Molecular Liquids,* vol. 437, p. 128396, 2025/11/01/ 2025, doi: https://doi.org/10.1016/j.molliq.2025.128396.

[17] M. Kaneda *et al.*, "Molecular Design of Functional Polymers for Silica Scale Inhibition," *Environmental Science & Technology,* vol. 58, no. 1, pp. 871-882, 2024/01/09 2024, doi: 10.1021/acs.est.3c06504.

[18] S. Ahmed, A. S. Maulud, M. Nawaz, and M. A. Bustam, "Evaluation and influence of ionic liquid functional group for leaching of yttrium oxide from ion adsorption clay," *Journal of the Indian Chemical Society,* vol. 103, no. 2, p. 102419, 2026/02/01/ 2026, doi: https://doi.org/10.1016/j.jics.2026.102419.

[19] M. S. Aminuddin, M. A. Bustam, and K. Johari, "Evaluation of amine-based ionic liquids as potential solvents for hydrogen sulfide absorption using COSMO-RS: Computational and experimental validation," *Chemical Engineering Research and Design,* vol. 203, pp. 721-730, 2024/03/01/ 2024, doi: https://doi.org/10.1016/j.cherd.2024.01.054.

[20] G. R. Choppin, P. Pathak, and P. Thakur, "Polymerization and complexation behavior of silicic acid: A review," *Main Group Metal Chemistry,* Review vol. 31, no. 1-2, pp. 53-71, 2008, doi: 10.1515/MGMC.2008.31.1-2.53.

[21] S. Ahmed Shahani, H. Warsi Khan, A. Mohd Shaiff, M. Goto, and M. Moniruzzaman,

"Screening of ionic liquids for the solubility enhancement of quinine using COSMO-RS," *Journal of Molecular Liquids,* vol. 409, p. 125388, 2024/09/01/ 2024, doi: https://doi.org/10.1016/j.molliq.2024.125388.

[22] A. Klamt and G. Schüürmann, "COSMO: a new approach to dielectric screening in solvents with explicit expressions for the screening energy and its gradient," *Journal of the Chemical Society, Perkin Transactions 2,* no. 5, pp. 799-805, 1993.

[23] H. A. Ahsan, M. A. Bustam, H. A. Murtaza, A. Mehmood, and B. Abdullah, "Process Simulation and Economic Evaluation of the [bmim][FeCl4] Ionic Liquid for H2S Direct Conversion to Elemental Sulfur," *ACS Omega,* 2026/07/08 2026, doi: 10.1021/acsomega.5c11851.

[24] Z. Wu *et al.*, "Ionic liquid screening for dichloromethane absorption by multi-scale simulations," *Separation and Purification Technology,* vol. 275, p. 119187, 2021/11/15/ 2021, doi: https://doi.org/10.1016/j.seppur.2021.119187.

[25] J. Afridi *et al.*, "Extraction of rare earth elements from ion adsorption clay using bio-based ionic liquid via COSMO-RS: Computational and experimental validation," *Journal of Rare Earths,* vol. 43, no. 10, pp. 2276-2284, 2025/10/01/ 2025, doi: https://doi.org/10.1016/j.jre.2024.11.002.

[26] M. Diedenhofen and A. Klamt, "COSMO-RS as a tool for property prediction of IL mixtures—A review," *Fluid Phase Equilibria,* vol. 294, no. 1, pp. 31-38, 2010/07/15/ 2010, doi: https://doi.org/10.1016/j.fluid.2010.02.002.

[27] H. C. Ting, H. W. Khan, A. V. B. Reddy, M. Goto, and M. Moniruzzaman, "Extraction of salicylic acid from wastewater using ionic liquid-based green emulsion liquid membrane: COSMO-RS prediction and experimental verification," *Journal of Molecular Liquids,* vol. 347, p. 118280, 2022.

[28] H. W. Khan *et al.*, "Exploring ionic liquids for formaldehyde separation via computational COSMO-RS screening," *Chemical Engineering Research and Design,* vol. 196, pp. 588-598, 2023/08/01/ 2023, doi: https://doi.org/10.1016/j.cherd.2023.06.055.

[29] H. Malik *et al.*, "Screening of ionic liquids as green entrainers for ethanol water separation by extractive distillation: COSMO-RS prediction and aspen plus simulation," *Chemosphere,* vol. 311, p. 136901, 2023.

[30] P. Davris, E. Balomenos, D. Panias, and I. Paspaliaris, "Leaching rare earth elements from bauxite residue using brønsted acidic ionic liquids," in *Rare earths industry*: Elsevier, 2016, pp. 183-197.

[31] F. Yang, T. Wu, T. Song, Q. Zhang, and Z. Zhang, "Separation of n-propanol - n-propyl acetate azeotropic system by extractive distillation with ionic liquids: COSMO-RS prediction, experimental investigation and quantum chemical calculation," *Journal of Molecular Liquids,* vol. 396, p. 124007, 2024/02/15/ 2024, doi: https://doi.org/10.1016/j.molliq.2024.124007.

[32] G. Ye, X. Wu, N. Gao, Y. Xu, Z. Guo, and X. Han, "COSMO-RS guided screening of ionic liquids for the separation of fluorinated greenhouse gases R-410A: Delving into anion, cation effects, and hydrogen bond dynamics," *Environmental Research,* vol. 239, p. 117386, 2023/12/15/ 2023, doi: https://doi.org/10.1016/j.envres.2023.117386.

[33] H. W. Khan *et al.*, "Evaluating ionic liquids for its potential as eco-friendly solvents for naproxen removal from water sources using COSMO-RS: Computational and experimental validation," *Environmental Research,* vol. 231, p. 116058, 2023.

[34] L. Zhou, Y. Liu, J. Zhang, Q. Li, M. Yuan, and Z. Kang, "Ionic liquid screening for lignocellulosic biomass fractionation: COSMO–RS prediction and experimental verification," *Journal of Molecular Liquids,* vol. 407, p. 125214, 2024/08/01/ 2024, doi: https://doi.org/10.1016/j.molliq.2024.125214.

[35] S. A. Shahani, W. Z. N. Yahya, M. Moniruzzaman, and M. H. Noh, "Rational Selection of Bio-Ionic Liquids for Zeaxanthin Solubilization: Computational Prediction to Biocompatibility Assessment," *ACS Sustainable Chemistry & Engineering,* vol. 14, no. 16, pp. 7599-7611, 2026/04/27 2026, doi: 10.1021/acssuschemeng.5c09924.

[36] H. W. Khan, A. V. B. Reddy, M. M. E. Nasef, M. A. Bustam, M. Goto, and M. Moniruzzaman,

"Screening of ionic liquids for the extraction of biologically active compounds using emulsion liquid membrane: COSMO-RS prediction and experiments," *Journal of Molecular Liquids,* vol. 309, p. 113122, 2020/07/01/ 2020, doi: https://doi.org/10.1016/j.molliq.2020.113122.

[37] C. Li, Y. Cao, B. Hu, and Y. Li, "Unraveling the effect of fluorine substitution on the hydrogen bonding interaction in the complexes of fluorosubstituted pyridines and acetic acid," *Journal of Physical Organic Chemistry,* Article vol. 34, no. 3, 2021, Art no. e4151, doi: 10.1002/poc.4151.

[38] Y. Q. Shi *et al.*, "Tethering Transition Metals of Li-Rich Manganese Oxides via Anion Coordination for High-Voltage Lithium-Metal Batteries," *Advanced Functional Materials,* Article vol. 36, no. 3, 2026, Art no. e14328, doi: 10.1002/adfm.202514328.

[39] H. W. Khan, A. A. Zailan, A. V. Bhaskar Reddy, M. Goto, and M. Moniruzzaman, "Ionic liquid-based dispersive liquid–liquid microextraction of succinic acid from aqueous streams: COSMO-RS screening and experimental verification," *Environmental Technology,* vol. 45, no. 19, pp. 3828-3839, 2024/08/23 2024, doi: 10.1080/09593330.2023.2234669.

[40] K. Binnemans, "Lanthanides and Actinides in Ionic Liquids," *Chemical Reviews,* vol. 107, no. 6, pp. 2592-2614, 2007, doi: 10.1021/cr050979c.

[41] D. Dupont and K. Binnemans, "Recycling of rare earths from NdFeB magnets using a combined leaching/extraction system based on the acidity and thermomorphism of the ionic liquid [Hbet][Tf2N]," *Green Chemistry,* vol. 17, no. 4, pp. 2150-2163, 2015, doi: 10.1039/c5gc00155b.